Onset of high-spin rotational bands in the $N = Z$ nucleus ^{62}Ga

D. Rudolph,[1,*] I. Ragnarsson,[1] S. Åberg,[1] C. Andreoiu,[1,2] M. P. Carpenter,[3] R. M. Clark,[4] J. Ekman,[1,5] C. Fahlander,[1] R. V. F. Janssens,[3,6] F. G. Kondev,[3] T. Lauritsen,[3] D. G. Sarantites,[7] D. Seweryniak,[3] and C. E. Svensson[8]

[1]*Department of Physics, Lund University, S-22100 Lund, Sweden*
[2]*Chemistry Department, Simon Fraser University, Burnaby, British Columbia, V5A 1S6, Canada*
[3]*Physics Division, Argonne National Laboratory, Argonne, Illinois 60439, USA*
[4]*Nuclear Science Division, Lawrence Berkeley National Laboratory, Berkeley, California 94720, USA*
[5]*Department of Material Science and Applied Mathematics, Malmö University, S-20506 Malmö, Sweden*
[6]*Department of Physics and Astronomy, University of North Carolina, Chapel Hill, North Carolina 27599, USA*
[7]*Chemistry Department, Washington University, St. Louis, Missouri 63130, USA*
[8]*Department of Physics, University of Guelph, Guelph, Ontario, N1G 2W1, Canada*

(Received 17 May 2020; accepted 25 June 2020; published 15 July 2020)

The fusion-evaporation reaction ^{28}Si + ^{40}Ca at 122 MeV beam energy was used to populate high-spin states in the odd-odd $N = Z$ nucleus ^{62}Ga. With the combination of the Gammasphere spectrometer and the Microball CsI(Tl) charged-particle detector array the decay scheme of ^{62}Ga was extended beyond 10 MeV excitation energy. The onset of band structures was observed. These high-spin rotational states are interpreted and classified by means of cranked Nilsson-Strutinsky calculations.

DOI: 10.1103/PhysRevC.102.014313

I. INTRODUCTION

Due to inherent symmetries, nuclei at or near the $N = Z$ line continue to be at the forefront of nuclear structure research. This includes, for instance, superallowed β decays, isobaric analog states identified by means of β-delayed proton emission, breaking of charge independence and charge symmetry in isospin $T = 1$ triplets or $T = 1/2$ mirror nuclei, or studying the influence of isovector $T = 1$ or isoscalar $T = 0$ pairing correlations on rotational behavior at high angular momenta. Beyond $N = Z = 28$ ^{56}Ni, the proton drip line is close to the $N = Z$ line, which often adds nuclear astrophysics aspects into mostly decay studies of $N \leqslant Z$ nuclei.

The odd-odd $N = Z$ nucleus ^{62}Ga is a well-studied example: a lot of effort has been put into precise measurements of details of the superallowed β decay of its $T = 1$, $I^\pi = 0^+$ ground state (see Refs. [1–3] and references therein). Triplet energy differences along the mass $A = 62$ isobars ^{62}Ge, ^{62}Ga, and ^{62}Zn have been studied, most recently by two-nucleon knockout [4]. This study provided evidence for the relevant $T = 1$, $I^\pi = 2^+$ state at 977 keV in ^{62}Ga, improving upon the results of Ref. [5], while both refine an earlier suggestion [6]. A β-decay study of ^{62}Ge reported a number of low-spin states in ^{62}Ga, all with tentative 1^+ assignments, including a state at 978 keV [7], while targeting the influence of $T = 0$ pairing correlations through weak Gamow-Teller decay branches. Similarly, ^{62}Ga is close to the borderline where odd-odd $N = Z$ nuclei change ground state from $T = 0$ to $T = 1$. This competition results in a crossing of the $T = 1$, $I^\pi = 0^+$ ground-state band by a $T = 0$ band already at spin $I = 2\,\hbar$.

The first medium- to high-spin states in ^{62}Ga were reported in Refs. [8–10]. These were extended based on studies employing multi-coincidence γ-ray spectrometers [5,6], identifying the odd-spin yrast sequence up to a terminating $I^\pi = 17^+$ state near 10 MeV excitation energy. For more complete experimental information we point to Ref. [11]. The possible rotational behavior of these states was subject of a dedicated theoretical study, discussing also $T = 0$ and $T = 1$ aspects [12]. However, different from most neighboring $A \approx 60$ nuclei [13,14], well- or superdeformed rotational bands have not yet been identified in ^{62}Ga. In particular, the odd-odd $N = Z$ neighbor ^{58}Cu enabled a case study, both experimentally [15–17] and theoretically [18–21]. There, comparisons with the 'doubly-magic superdeformed band' in ^{60}Zn [13] as well as possible influences of neutron-proton pairing correlations in the isospin $T = 0$ or $T = 1$ channels were investigated.

Revisiting existing data from experiments briefly described in Sec. II, we present an analysis devoted to high-spin states in ^{62}Ga as outlined in Sec. III. The experimental results are presented in Sec. IV. The newly observed structures, indicating the onset of the long-sought well-deformed rotational bands in ^{62}Ga, are discussed in Sec. V and compared with results from cranked Nilsson-Strutinsky calculations. The paper concludes with a brief summary.

II. EXPERIMENT

The experiment was conducted at the Argonne Tandem Linac Accelerator System (ATLAS). The fusion-evaporation

*Dirk.Rudolph@nuclear.lu.se

reaction ^{28}Si + ^{40}Ca, at a beam energy of 122 MeV, was used to populate high-spin states in neutron-deficient, mass $A \approx 60$ nuclei near the $N = Z$ line. Excited states in ^{62}Ga were reached following the evaporation of one α particle, one proton, and one neutron, i.e., the $1\alpha 1p1n$ reaction channel. An experimental relative production cross section of $\sigma_{\rm rel} \approx 0.2\%$ could be estimated. The ^{40}Ca target was enriched to 99.975% and 0.5 mg/cm^2 thin. It was enclosed by two thin gold layers and transported to the target chamber in argon atmosphere to prevent oxidation.

The experimental setup combined the Gammasphere array [22] surrounding the target chamber with the nearly 4π 95-CsI(Tl)-element charged-particle detector system Microball [23] inside. At the time of the experiment, Gammasphere comprised 101 germanium detector elements. The heavimet collimators were removed from the detector elements to allow for γ-ray multiplicity and γ-ray sum-energy measurements [24]. In conjunction with the summed energies of the evaporated charged particles measured with Microball, this information is useful for reaction channel selection [25]. Events were recorded when at least four Compton-suppressed γ rays were detected.

III. DATA ANALYSIS

The data analysis follows procedures established and described earlier a number of times in extensive studies of neighboring nuclei for this and similar experiments in the mass $A \approx 60$ region [26–30]. In brief, based on momenta of evaporated charged particles measured with Microball, the momenta of the recoiling residues can be derived on an event-by-event basis. In combination with a number of twofold segmented germanium detectors around central angles in Gammasphere, this allows for more accurate Doppler-shift corrections and thus significantly improved γ-ray energy resolution.

^{62}Ga is a relatively weakly populated reaction channel involving neutron evaporation, here $1\alpha 1p1n$, from the compound nucleus ^{68}Se. Therefore, channel selection is crucial for extracting the information necessary to reliably construct the level scheme. Usually, active detection of evaporated neutrons in prompt coincidence with the γ rays is a must (see, e.g., Ref. [15]). Alternatively, recoil-γ coincidence spectroscopy can be employed (see, e.g., Ref. [5]). In addition, either one or both types of selection schemes can be combined with the total-energy methods mentioned earlier [25].

Interestingly, it is possible to discriminate the weak $1\alpha 1p1n$ channel ^{62}Ga in the present data set, though neither having neutron detectors in the setup nor recoil-γ coincidences enabled. The three γ rays connecting the $5^+ \rightarrow 3^+ \rightarrow 1^+ \rightarrow 0^+$ low-spin yrast sequence, namely at 377, 246, and 571 keV [11], can be used to tag ^{62}Ga. Of course, this is done in combination with the standard requirement of prompt coincidences with one α particle and one proton detected in Microball. The reason is that the γ-ray spectra in coincidence with any of these three transitions contain no more than 5–10 % contamination from any of the much more intensely populated reaction channels leaking into the $1\alpha 1p$ data due to missing the detection of one or more evaporated protons or α particles, respectively. The high-spin level schemes of the

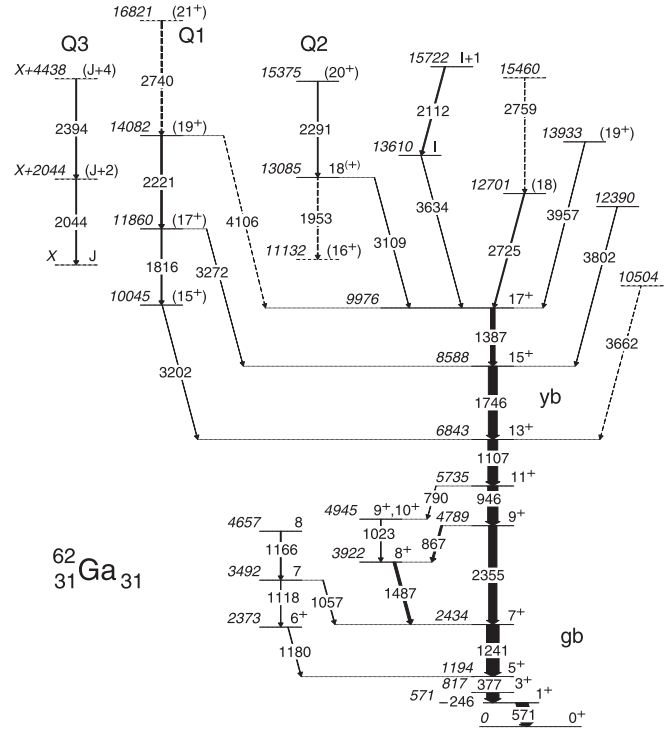

FIG. 1. Proposed level scheme of ^{62}Ga from the present study. Energy labels are in keV. Tentative transitions and levels are dashed. The widths of the arrows correspond to the relative intensities of the γ rays. In the figure, $X = 11$ MeV.

contaminating reaction channels, including ^{62}Zn ($1\alpha 2p$, [30]), ^{61}Cu ($1\alpha 3p$, [27]), ^{61}Zn ($1\alpha 2p1n$, [28]), ^{59}Cu ($2\alpha 1p$, [26]), or ^{58}Ni ($2\alpha 2p$, [29]), are all very well known, likewise the $1\alpha 1p$ channel ^{63}Ga [31]. The γ-ray spectra in coincidence with any combination of the three low-lying transitions in ^{62}Ga reveal almost exclusively lines associated with ^{62}Ga (see Sec. IV). In an iterative process, this fact was used to optimize the conditions on event-by-event γ-ray multiplicity as well as γ-ray sum-energy and total-energy measurements [24,25] to obtain the best possible signal-to-contamination ratio for the analysis of excited states in ^{62}Ga in the preselected $1\alpha 1p$ data set.

With the $1\alpha 1p$ coincidence, and the mentioned optimized conditions, the subsequent γ-ray analysis steps involved E_γ projections, E_γ-E_γ matrices, and an E_γ-E_γ-E_γ cube. These were inspected by means of the RADWARE software package [32] and the spectrum-analysis code TV [33]. E_γ projections and E_γ-E_γ matrices required a coincidence with at least one of the three low-energy γ-ray transitions at 246, 377, or 571 keV. The inspection of the E_γ-E_γ-E_γ cube engaged almost always one or more of these three transitions as well. The analysis resulted in the experimental high-spin level scheme of ^{62}Ga shown in Fig. 1. The selectivity for ^{62}Ga can be judged by the γ-ray spectrum displayed in Fig. 2(a).

Well-deformed rotational bands in the $A \approx 60$ region involve typically γ-ray transitions between some 1.5 and 4.0 MeV. The lifetimes of the corresponding states are usually so short that the residual nuclei emit these γ rays while the nucleus is still inside the thin target layer, i.e. moving with slightly higher velocities than used for standard Doppler

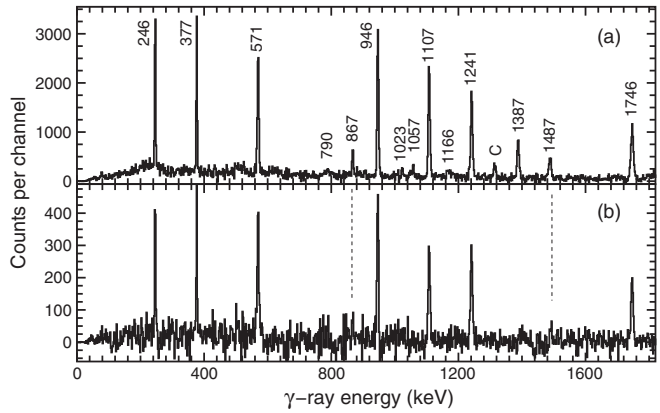

FIG. 2. γ-ray spectra related to the main yrast structure of ^{62}Ga shown in Fig. 1. Besides the preselection for the analysis of ^{62}Ga residues described in Sec. III, the spectrum in (a) is in coincidence with any of the two 246- or 377-keV transitions, selecting ^{62}Ga, and, in addition, any of the 246-, 377-, 571-, or 1241-keV transitions known to belong to the low-spin yrast sequence of ^{62}Ga. The spectrum in (b) is in coincidence with either the 246- or 377-keV transition and the 1387-keV $17^+ \rightarrow 15^+$ yrast transition. Energy labels are in keV. The binning is 2 keV per channel. The mark 'C' indicates a transition, which arises from a tiny $\gamma\gamma\gamma$ contamination involving the 1310-1317-keV ground-state sequence in ^{61}Cu.

corrections adopted for γ-ray transitions in the lower part of the level scheme, once the residues left the target layer. With sufficient statistics, these additional Doppler shifts of transitions connected to well-deformed rotational bands can be used to derive quadrupole moments, Q_t, of the bands (see Ref. [26] for an example). Based on assumed average quadrupole moments typical for the $A \approx 60$ region, one can apply a generic additional Doppler-shift correction to improve the energy resolution for γ rays originating from rotational bands, at the cost of slightly worsening the energy resolution for γ rays connecting low-lying states of the level schemes. For the present analysis and in view of the established part of the level scheme in Fig. 1 [11], this was implemented for the range $E_\gamma = [1760, 4000]$ keV. Such an '$F\tau$-corrected' E_γ-E_γ matrix and E_γ-E_γ-E_γ cube were inspected as well.

Assignments of spins and parities of the excited levels were based on the analysis of the $1\alpha 1p$-gated directional E_γ-E_γ correlations of oriented states (DCO ratios). The Ge detectors of Gammasphere were grouped into two 'pseudo' rings called '30' and '83', which correspond to an average angle for the respective set of detectors while accounting for γ-ray emission symmetry with respect to the 90°-plane perpendicular to the beam. The DCO matrix considered was once again preselected by requiring a coincidence with at least one of the three low-energy γ-ray transitions at 246, 377, or 571 keV, which could be detected in any detector at any angle of the Gammasphere spectrometer. The remaining γ rays detected at 30° were sorted on one axis and those detected at 83° placed on the other axis of the DCO matrix.

DCO ratios were then derived according to

$$R_{\mathrm{DCO}}(30\text{-}83) = \frac{I(\gamma_1 \text{ at } 30^\circ; \text{gated with } \gamma_2 \text{ at } 83^\circ)}{I(\gamma_1 \text{ at } 83^\circ; \text{gated with } \gamma_2 \text{ at } 30^\circ)}.$$

Known stretched $E2$ transitions above the 1194-keV 5^+ state were used for gating. In this case one expects $R_{\mathrm{DCO}}(30\text{–}83) = 1.0$ for observed stretched $E2$ transitions and $R_{\mathrm{DCO}}(30\text{–}83) \approx 0.6$ for stretched pure $\Delta I = 1$ transitions. Deviations from the estimates for pure $\Delta I = 1$ transitions indicate a non-zero mixing ratio of the respective transition, namely $\delta(E2/M1) > 0$ (< 0) for numbers smaller (larger) than expected for $R_{\mathrm{DCO}}(30\text{–}83)$. Nonstretched $\Delta I = 0$ transitions yield typically $R_{\mathrm{DCO}}(30\text{–}83) \approx 0.9$, i.e., numbers similar to stretched $E2$ transitions. Since the γ-ray decay paths in nuclei populated via fusion-evaporation reactions follow the yrast line, $\Delta I = 0$ transitions are rare and usually have small relative intensities.

For the present data set, the required selection of ^{62}Ga events based on its ground-state γ-ray cascade prevents sensitivity for prompt particle emission from high-spin rotational states [15,29]. However, prompt proton emission is unlikely because all well- or superdeformed high-spin bands observed in the daughter nucleus ^{61}Zn could be connected into low-spin states of ^{61}Zn [28]. Similarly, in the decay scheme of ^{58}Cu, no indication of any prompt α emission from states in ^{62}Ga could be identified.

The collaboration conducted also a series of high-spin experiments with Gammasphere producing the compound nucleus ^{64}Ge, populating ^{62}Ga in the $1p1n$ channel. If one were to discriminate ^{62}Ga events in these data sets, one might expect to populate very high spin states. Though such an approach worked out nicely for the $2p$ channel ^{62}Zn [34] (and, similarly in yet another data set, for ^{58}Ni populated via $2p$ evaporation [35]), it did not yield any results for ^{62}Ga. The explanation can be found in the low absolute and relative production cross-section for the $1p1n$ vs $2p$ reaction channel.

IV. EXPERIMENTAL RESULTS

The level scheme derived from the present study is shown in Fig. 1. The yrast sequence up to the 17^+ state at 9976 keV and the off-yrast part between 2 and 5 MeV excitation energy was reported previously [4–6,9,10], the latter in fact more comprehensively. This is readily understood in terms of anticipated entry-state distributions, which are shifted to on average higher excitation energies and larger angular momenta for the present data set. The only minor inconsistency with previous work is the γ-ray energy reported for the $17^+ \rightarrow 15^+$ transition, being 1390 keV in Ref. [5] but 1387.9(10) keV in Ref. [9] and here found to be 1387.4(7) keV. All states beyond an excitation energy of 10 MeV and the γ rays connected to them were observed for the first time.

Energies and spin-parity assignments of the levels in the decay scheme of Fig. 1 as well as energies, relative intensities, and DCO ratios of the transitions are summarized in Table I. The intensities are normalized to the 1241-keV, $7^+ \rightarrow 5^+$ transition, since the three γ-ray lines below the 1194-keV 5^+ state were used to select the nucleus of interest. Obviously, up until the 1746-keV $15^+ \rightarrow 13^+$ transition the γ-ray flux is well confined and collected in the yrast structure, while it fragments over an increasingly large number of transitions beyond some 9 to 10 MeV excitation energy.

TABLE I. The energies of excited states in ^{62}Ga, the transition energies and relative intensities of the γ rays placed in the level scheme, their DCO ratios and multipole assignments, and the derived spins and parities of the initial and final states connected by the γ rays.

E_x (keV)	E_γ (keV)	I_{rel} (%)	Gate[a]	R_{DCO} 30°–83°	Mult. Ass.	I_i^π ($\hbar$)	I_f^π ($\hbar$)
570.7(3)	570.7(3)	100[b]			$M1$[c]	1^+	0^+
816.8(3)	246.1(2)	100[b]			$E2$[c]	3^+	1^+
1193.6(4)	376.8(2)	100[b]			$E2$[c]	5^+	3^+
2373.4(8)	1179.8(8)	4.7(8)			$E2/M1$[c]	6^+	5^+
2434.4(6)	1240.9(5)	100.0(35)[d]	B	1.07(10)	$E2$	7^+	5^+
3491.8(8)	1057.3(7)	5.4(5)			$\Delta I = 0$[c]	7	7^+
	1118.3(8)	3.8(7)			$\Delta I = 1$[c]	7	6^+
3921.9(8)	1487.4(6)	21.1(10)	C	0.69(15)	$E2/M1$	8^+	7^+
4657.4(11)	1165.7(8)	7.4(5)			$\Delta I = 1$[c]	8	7
4789.2(8)	867.3(4)	15.0(7)	C	0.39(9)	$E2/M1$	9^+	8^+
	2354.8(9)	65.5(25)	B	1.16(13)	$E2$	9^+	7^+
4944.9(9)	1022.9(5)	4.6(4)				$9^+, 10^+$	8^+
5735.3(9)	790.2(7)	3.4(5)				11^+	$9^+, 10^+$
	946.2(4)	81.6(29)	B	1.01(9)	$E2$	11^+	9^+
6842.7(10)	1107.4(5)	77.9(28)	B	1.04(9)	$E2$	13^+	11^+
8588.4(13)	1745.8(8)	70.4(26)	A	1.03(11)	$E2$	15^+	13^+
9975.9(14)	1387.4(7)	36.1(14)	A	1.09(13)	$E2$	17^+	15^+
10044.6(19)	3201.6(21)	3.1(8)	A	≈1	$(E2)$	(15^+)	13^+
10504.3(33)	3661.6(31)	1.4(3)					13^+
11860.4(20)	1815.7(14)	8.4(4)	A	1.19(53)	$(E2)$	(17^+)	(15^+)
	3271.8(27)	1.6(3)			$(E2)$[e]	(17^+)	15^+
12390.1(28)	3801.6(25)	3.5(6)					15^+
12701.0(23)	2725.1(18)	8.5(7)	B	0.71(21)	$(\Delta I = 1)$	(18)	17^+
X+2044	2043.9(17)	7.0(4)	B	1.25(50)	$(E2)$	$(J+2)$	J
13084.9(25)	1953.3(17)	6.6(4)			$(E2)$[f]	$18^{(+)}$	(16^+)
	3109.0(20)	3.2(4)	B	0.37(26)	$(E2/M1)$	$18^{(+)}$	17^+
13610.1(28)	3634.2(24)	2.7(4)				I	17^+
13932.8(30)	3956.9(26)	3.1(3)	B	1.0(6)	$(E2)$	(19^+)	17^+
14081.5(22)	2221.0(17)	12.5(7)	B	0.88(24)	$(E2)$	(19^+)	(17^+)
	4106.2(29)	0.9(2)			$(E2)$[e]	(19^+)	17^+
15375.4(29)	2290.5(15)	6.4(5)			$(E2)$[f]	(20^+)	$18^{(+)}$
X+4438	2393.6(16)	7.6(4)	B	1.02(34)	$(E2)$	$(J+4)$	$(J+2)$
15459.7(29)	2758.7(18)	3.3(3)					(18)
15722.1(31)	2112.0(14)	9.8(5)	B	0.50(23)	$\Delta I = 1$	$I+1$	I
16821.1(38)	2739.6(31)	4.1(11)			$(E2)$[f]	(21^+)	(19^+)

[a]A: 945, 1107, 1241, and 2355 keV; B: 945, 1107, 1241, 1387, 1746, and 2355 keV; C: 945, 1107, 1241, 1387, and 1746 keV.
[b]Intensity set to $I_{rel} = 100$ due to the isomeric character of the 817-keV 3^+ state, which also prevents the derivation of a DCO ratio.
[c]Multipolarities and spin-parity assignments taken from earlier low- to medium-spin state studies [4–6,10].
[d]Relative intensity normalized to $I_{rel} = 100.0(35)$.
[e]Tentative multipolarity assignments based on spin difference between initial and final levels.
[f]Tentative multipolarity assignments based on rotational character and yrast arguments.

The γ-ray spectra in Fig. 2 provide the low-energy reference spectrum for ^{62}Ga in panel (a) and the confirmation of the 1387-keV line concluding the yrast sequence up to the 17^+ state at 9976 keV in panel (b). The yrast sequence includes the bypass via the 3922-keV 8^+ state, while panel (a) reveals also several of the γ rays known to belong to the low-spin nonyrast structure of ^{62}Ga. The one, and only notable contamination, in the spectrum in Fig. 2(a), marked 'C', is at 1310 keV, which corresponds to the energy of the most intense transition in ^{61}Cu [27]. The DCO ratios of the 1387-1746-1107-946-2355-1241-keV sequence are all in agreement with stretched $E2$ multipolarity, which in combination with yrast arguments allows for firm spin and parity assignments of the concerned states. The DCO ratio of the 1487-keV transition points to a $\Delta I = 1$ assignment, while the DCO value for the 867-keV transition is clearly below 0.6, i.e., it has a finite $E2/M1$ mixing ratio, i.e., the spin $I = 8$ state at 3922 keV must have positive parity. Due to yrast arguments, the state at 4945 is likely to be the yrare 9^+ state, while technically a 10^+ assignment cannot be excluded. Due to two γ rays bridging three units of angular momentum between the 5735- and 3922-keV states, the parity of the 4945-keV state must be positive though. Spin-parity assignments of the 2373-3492-4657-keV side structure were taken from Refs. [5,6].

The γ-ray spectrum in Fig. 3 is the basis for the newly observed high-spin part of the level scheme in Fig. 1. It shows

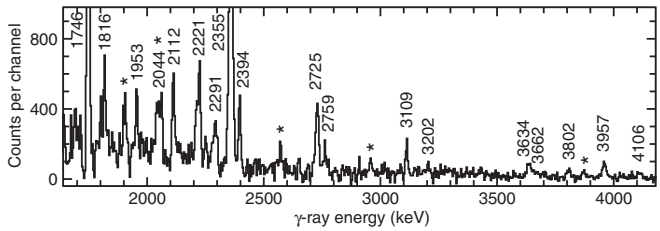

FIG. 3. High-energy part of a γ-ray spectrum taken in coincidence with any of the two 246- or 377-keV transitions and in combination with any of the other transitions in the main yrast sequence of ^{62}Ga up to the 9976-keV 17^+ state, namely γ rays at 246, 377, 571, 867, 946, 1107, 1241, 1387, 1487, 1746, or 2355 keV. The binning is 4 keV per channel. Transitions marked with a '$\star$' could either not be placed in the decay scheme of ^{62}Ga or relate to a small $\gamma\gamma\gamma$ contamination from other, much more intensely populated reaction channels.

the relevant high-energy part of the sum of all spectra taken in coincidence with any combination of the three low-energy transitions (246, 377, or 571 keV) and all those spectra in coincidence with any of these three transitions and with any of the other transitions in the yrast sequence (867, 946, 1107, 1241, 1387, 1487, 1746, or 2355 keV). For the spectrum in Fig. 3, the '$F\tau$ correction' was applied (cf. Sec. III).

Sum-energy and individual coincidence relations give rise to the 10045-11860-14082 rotational-like sequence. With $I_{\rm rel} = 12.5\%$ the 2221-keV transition is the most intense one identified in this part of the level scheme. A possible continuation of the 1816-2221-keV band was found at 2740 keV. Notably, the 3202-, 3272-, and the tentative 4106-keV linking transitions do not carry the full γ-ray flux back into the yrast sequence. This is typical for the mass region, i.e., the observation of links but not a full accounting for the decay path—besides the exceptional case study of the decay-out from the yrast superdeformed band in ^{59}Cu [36]. DCO ratios of the 3202-, 1816-, and 2221-keV transitions are indicative of $E2$ character, which in conjunction with intensity arguments can be used to provide tentative spin-parity assignments for that band.

In turn, the 3109-keV transition is found to be of dipole character, giving rise to a $18^{(+)}$ assignment of the 13085-keV state, which is fed by the 2291-keV transition and possibly depopulated by a 1953-keV transition. Similarly, the somewhat weaker 2044-2394-keV transitions are found to be in mutual coincidence. However, no connection to the main part of the level scheme could be resolved. Since $(1816 + 2221)/2 \approx 2044$ and $(2221 + 2740)/2 \approx 2394$, this sequence has been placed at $X = 11000$ keV (and implicitly $J = 16$), indicative for another possible signature partner of the 1816-2221-2740-keV structure. The DCO ratios for both the 2044- and 2394-keV transitions are consistent with stretched $E2$ nature.

Somewhat surprisingly, the 2112-keV line is found to have stretched dipole character, i.e., it is of either stretched $M1$ or $E1$ character. It connects via the 3634-keV high-energy transition into the 9976-keV level. Similarly, the DCO ratio of the 2725-keV line, feeding that level as well, points towards a dipole assignment. The cube analysis indicates that the weak 2759-keV line should be placed on top of the 12701-keV state. These two sequences do not indicate well-deformed rotational bands. Finally, three more high-energy γ-rays at 3662, 3802, and 3957 keV are found to feed the 13^+, 15^+, and 17^+ yrast states, respectively. Whether or not they represent links to deformed rotational bands remains open at the present level of available statistics.

Clearly, the level scheme in Fig. 1 runs out at some 16 MeV excitation energy and an angular momentum of some 20 $\hbar$. This is comparable to the high-spin studies of neighboring odd-odd $N = Z$ nuclei populated through similar fusion-evaporation reactions. The high-spin scheme of ^{58}Cu extends to somewhat larger values of excitation energy and spin, probably due to the presence of one dominating rotational band [15,16]. The interpretation of ^{54}Co at high spins implies that the γ-ray flux is spread out over many possible deformed bands [37]. The high-spin region in ^{66}As remains to be settled [38,39].

V. DISCUSSION

The cranked Nilsson-Strutinsky (CNS) calculations are based on the modified oscillator potential, which is cranked around a principal axis [40–42]. Here, we consider both the standard parameters [40] and the prescriptions and new Nilsson parameters for the mass $A \approx 60$ region derived more recently [43].

Active j shells comprise the complete $\mathcal{N} = 3$ oscillator shell as well as $1g_{9/2}$ in the $\mathcal{N} = 4$ oscillator shell. CNS configurations are classified by the number of holes in the $1f_{7/2}$ orbital and particles in either the upper fp or $1g_{9/2}$ orbitals. Note, however, that in CNS, we do not refer to the pure j shells but rather to the orbitals in the deformed rotating potential which have their dominant amplitudes in these j shells. The CNS notation $[(p_1)p_2p_3;(n_1)n_2n_3]$ is used where p_1 (n_1) represents the number of proton (neutron) holes in orbitals of $f_{7/2}$ character, p_2 (n_2) the number of protons (neutrons) of fp character, and p_3 (n_3) the number of $g_{9/2}$ protons (neutrons). Labels in parentheses are omitted when equal to zero. For an odd number of particles, signature might be specified as subscript index '+' or '−', for example, $[21_+, 21_+]$.

For an extensive study of ^{62}Ga up to the 9976-keV 17^+ state, including isospin aspects within shell-model and CNS approaches, we refer to Ref. [12]. Here, we focus on the hitherto unobserved states at high spin, which indicate the onset of well-deformed rotational structures in ^{62}Ga.

The CNS description started with a scan for the yrast states for the four combinations of parity, $\pi = +, -$, and signature, $\alpha = 0, 1$ for angular momenta up to spin $I = 30\hbar$. These results are shown in Fig. 4. At low spin, the yrast states are expected, and found to have, all valence particles in the fp orbitals, corresponding to CNS configurations of the type $[30;30]$. For a brief spin interval, 9^- and 11^- negative-parity, $\alpha = 1$ states form the yrast line, i.e., with only one particle in the lowest $g_{9/2}$ Nilsson orbital, $[21_+;3_+0]$. Up to the terminating 17^+ state, the symmetric $[21_+, 21_+]$ configuration is predicted to form a distinct signature $\alpha = 1$ yrast sequence. One can recall that the signature splitting for

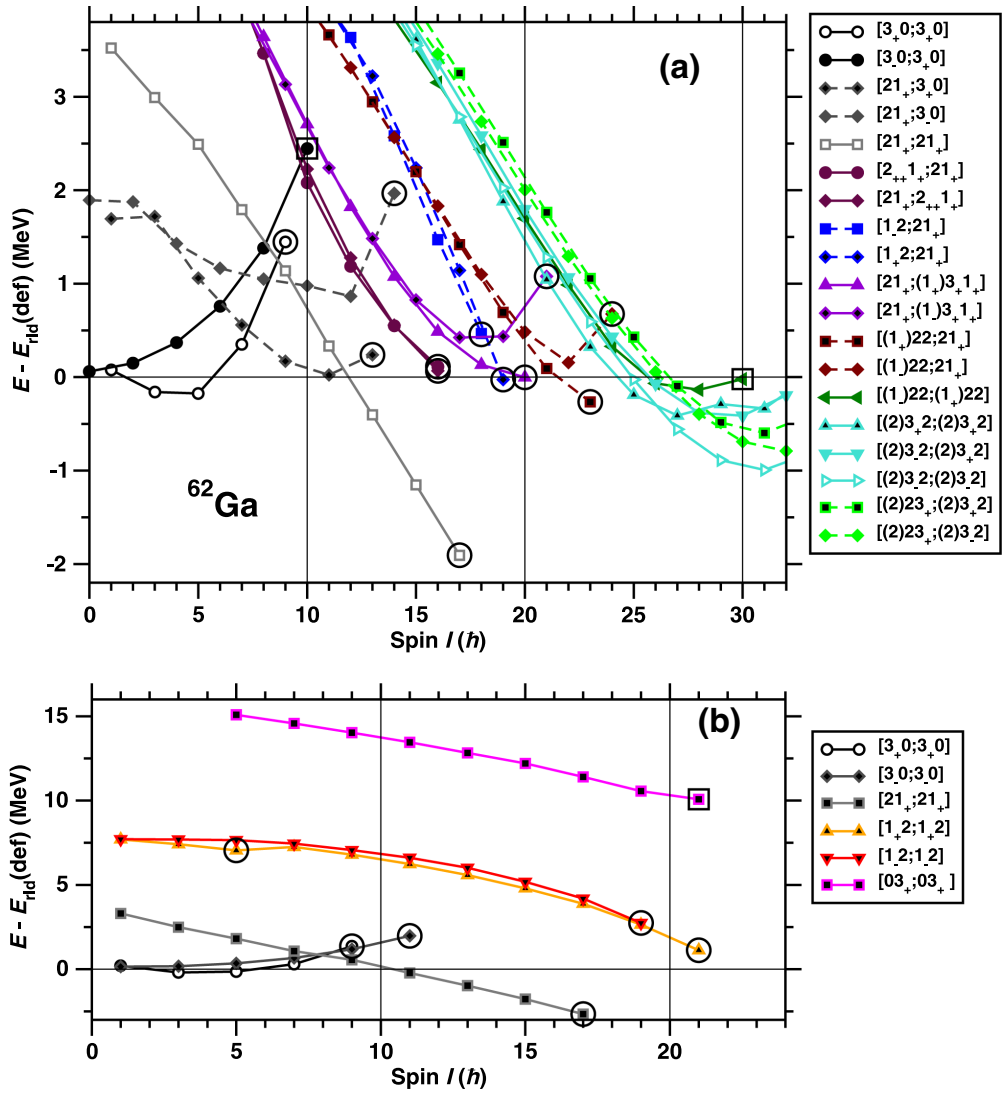

FIG. 4. (a) shows typical examples for different classes of predicted bands. They are obtained from a scan for yrast configurations for the four combinations of parity and signature for spins up to $I = 30\hbar$ in ^{62}Ga, using standard CNS parameters [40]. They are plotted relative to a rotating liquid drop energy, E_{rld}, calculated according to Ref. [44]. Positive (negative) parity is indicated by straight (dashed) lines. Signature $\alpha = 0$ ($\alpha = 1$) is indicated by filled (open) symbols). Large open circles indicate noncollective states, i.e., where the spin is built from 'rotation around the symmetry axis'. Large squares are used for states which have reached their I_{max} values though still more or less collective. (b) shows proton-neutron symmetric configurations of ^{62}Ga of types $[3_+0;3_+0]$, $[3_-0;3_-0]$, $[21_+;21_+]$, $[1_+2;1_+2]$, $[1_-2;1_-2]$, and $[03_+;03_+]$, i.e., without considering holes in $f_{7/2}$ orbitals. These CNS calculations use the new parameters [43].

the lowest $g_{9/2}$ orbital is so large that for signature $\alpha = 0$, i.e., even spin values, it is more favorable to let either the two fp protons or the two fp neutrons have the same signature (cf. $[2_{++}1_+;21_+]$ or $[21_+;2_{++}1_+]$ in Fig. 4) than converting one $g_{9/2}$ from signature $\alpha = +1/2$ into signature $\alpha = -1/2$, corresponding to, e.g., the $[21_-;21_+]$ configuration.

To obtain spin values in excess of $I = 17\,\hbar$ it is possible to stay in the valence space and lift a third particle from the fp into the $g_{9/2}$ orbitals. Two such negative-parity configurations, $[1_-2;21_+]$ and $[1_+2;21_+]$ show a favored termination close to (18^-) or at yrast (19^-), respectively. More interesting, however, are configurations that involve an additional hole in $f_{7/2}$, i.e., of type $[(1)31;21]$ or $[21;(1)31]$, respectively. Two bands of this type are shown in Fig. 4(a), which terminate at spins $I = 20$ and $21\,\hbar$, respectively. One can note that the termination at $I = 21\hbar$ is very much unfavored compared with the band terminating at spin $20\hbar$. In line with investigations in ^{62}Zn (cf. discussion of the bands TB1 and TB2 in Ref. [30]), it is known that the signature change of a hole in $f_{7/2}$ (e.g., from $[21_+;(1_+)3_+1_+]$ to $[21_+;(1_-)3_+1_+]$) is costly in excitation energy.

For the sake of the observed states displayed in Fig. 1, one could stop here. Nevertheless, we note that the next predicted excitation is to switch to negative parity bands by lifting a third fp particle into a $g_{9/2}$ orbital before configurations with four holes in $f_{7/2}$ and four or five particles in $g_{9/2}$ orbitals dominate the yrast line at $I \approx 30\hbar$. In fact, the configuration $[(2)32;(2)32]$ relate ^{62}Ga at high spins to the anticipated $[(2)22;(2)22]$ configuration of the superdeformed band observed in ^{60}Zn [13,18,20].

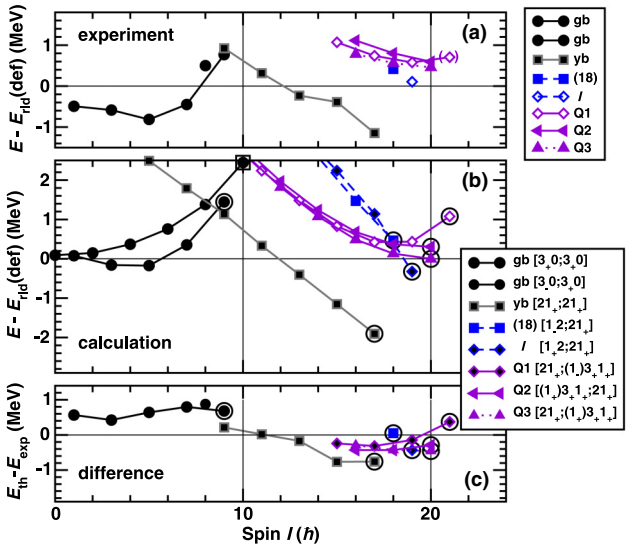

FIG. 5. (a) shows energies relative to the rotating liquid drop energy [44] of the observed 'bands' in ^{62}Ga They are compared with the assigned calculated CNS configurations using standard parameters [40] in (b). The difference between experiment and theoretical interpretation is shown in (c). The label 'gb' represents the $\pi(fp)^3\nu(fp)^3$ ground band up to spin 9^+, denoted $[3_+0;3_+0]$ in the CNS description. Moving one proton and one neutron into the lowest $g_{9/2}$ orbitals leads to the $[21_+;21_+]$ band labeled 'yb'. High-spin bands Q1, Q2, and Q3 are interpreted to involve the excitation of either one proton or one neutron across the shell gap at particle number 28. Connections of experiment-related data points of Q3 are dotted due to the unknown excitation energy ($X \approx 11$ MeV in Fig. 1). The data point at spin $I = 21\hbar$ in Q1 is tentative, hence put in parentheses.

It is instructive to consider the proton-neutron symmetric configurations in ^{62}Ga with an increasing number of $g_{9/2}$ particles, which are shown in Fig. 4(b). As already noticed in Fig. 4(a), the configurations with no or one such proton and neutron are calculated yrast, and the latter turns out to be particularly favored. Also the configurations with two $g_{9/2}$ particles approach the yrast line for their terminating states at $I = 20$ and $21\,\hbar$, respectively. However, the band with all valence particles in $g_{9/2}$ orbitals lies high above yrast over its full spin range. This is different from the $I = 21\hbar$ state in ^{94}Ag with all six valence holes in $g_{9/2}$ orbitals, which appears to be particularly favored in energy [45]. The difference is, of course, that with particles outside the $N = Z = 28$ gap there is a competition to put the valence particles in either the fp orbitals or the $g_{9/2}$ orbitals while holes in the $N = Z = 50$ core are naturally put in the $g_{9/2}$ orbitals because the competing $\mathcal{N} = 3$ shells are much lower in energy.

Figures 5 and 6 provide the comparison of the experimental bands and CNS calculations with standard [40] and new $A \approx 60$ [43] parameters. Following up on the discussion in Ref. [12], it is obvious that the experimental signature $\alpha = 1$, 1^+ through 9^+ sequence (571- through 4789-keV levels) should be assigned to the $[3_+0;3_+0]$ CNS configuration. The level of agreement is within 1 MeV, expected and typical for such low-spin states, and of comparable size for the two parametrizations. The experimental 3922-keV 8^+ state finds its counterpart in a corresponding $\alpha = 0$ configuration. It lies above the spin 1 to 9 sequence in both experiment and calculations.

The assignment of the experimental signature $\alpha = 1$, 9^+ through 17^+ sequence (4945- through 9976-keV levels) to the $[21_+;21_+]$ CNS configuration is also apparent [12]. Looking at details, the kink in the experimental data at spin $I = 13\hbar$ suggests a switch from a $p^2_{3/2}\,g_{9/2}$ occupation for both protons and neutrons ($I_{\max} = 13\hbar$) to a different $(fp)^2\,g_{9/2}$ occupation for both protons and neutrons ($I_{\max} = 17\hbar$). In fact, the $8^+ \to 6^+ \to 4^+ \to 2^+ \to 0^+$ cascade in the even-even core ^{60}Zn reveals an almost identical behavior [13]. In a seniority coupling scheme, the proton and neutron in the $g_{9/2}$ orbital can be viewed as an aligned spectator contributing with $I = 9\hbar$ with seniority $\nu = 2$. Seniority $\nu = 4$ states reach a maximum of $I = (9+4)\hbar = 13\hbar$ (for this $\alpha = 1$ band). Breaking an additional pair, i.e., switching to seniority $\nu = 6$, provides the remaining states with $I_{\max} = (9+4+4)\hbar = 17\hbar$. In this picture, the change in seniority explains the kink in energy observed experimentally in Fig. 5(a) [12].

For the predicted negative-parity yrast 9^- and 11^- states there are neither candidates in the present data nor reported in earlier medium-spin studies [5,6]. At lower spins, the corresponding structures are quickly becoming nonyrast. Population from the top, i.e., via the signature $\alpha = 1$ positive parity yrast sequence, is very unlikely, because it would require $M2$ transitions between, for instance, the observed 13^+ and the predicted 11^- yrast states. Note that the negative-parity states with signature $\alpha = 0$ never turn yrast in this spin region due to too large a signature splitting even in the fp orbitals (cf. Fig. 4).

Moving beyond spin $I = 17\hbar$, another excitation from an fp into a $g_{9/2}$ orbital invokes rotational bands concluding in favored termination. The experimental level at 12701 keV with a tentative spin 18 assignment is a good candidate to match the predicted 18^- terminating state of the $[1_-2;21_+]$ configuration. An experimental candidate for the predicted terminating 19^- state of the $[1_+2;21_+]$ configuration might be the level at 13610 keV. Here, the strength of a high-energy 3634-keV line could account for the intrinsically required $g_{9/2} \to f_{5/2}\,M2$ recoupling to reach the terminating 17^+ state of the $[21_+, 21_+]$ configuration.

The rather short bands observed above $I = 17\hbar$, labeled Q1, Q2, and Q3 in Fig. 1, are in good agreement with the CNS configurations involving either a proton or neutron excitation from a $f_{7/2}$ orbital into a fp orbital, i.e., one hole in the $f_{7/2}$ shell. These bands are of the same type as the first smoothly terminating bands which were identified in the $A = 60$ region, namely bands with one hole in the $f_{7/2}$ in ^{64}Zn [46] and ^{62}Zn [47]. For ^{62}Ga, if one assumes that the Q3 band is similar to the Q2 band (but slightly lower in energy than plotted in Fig. 1), the difference between experiment and calculations in Figs. 5(c) and 6(c) is essentially constant as a function of spin and close to zero. The only deviation is found for the tentative $21^+ \to 19^+$ transition, for which experiment suggests a less unfavored termination as the predictions. As discussed above, the unfavored energy is caused by a large signature splitting at termination for configurations with one hole in the $f_{7/2}$ shell which in turn is understood from the high energy cost to make

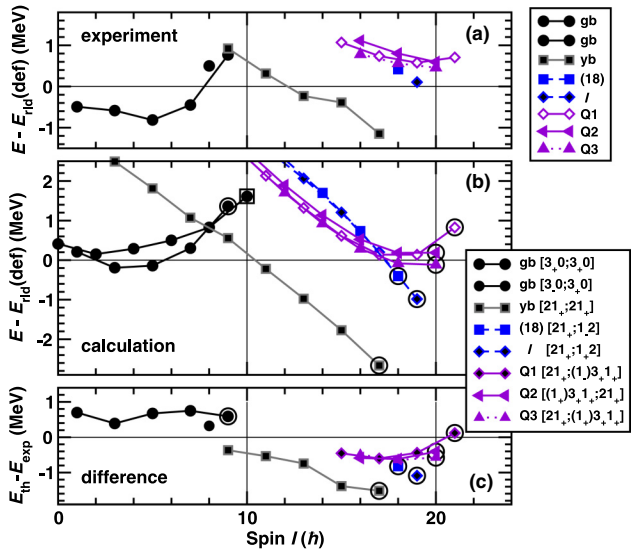

FIG. 6. Same as Fig. 5 but using new parameters [43] for the CNS calculations.

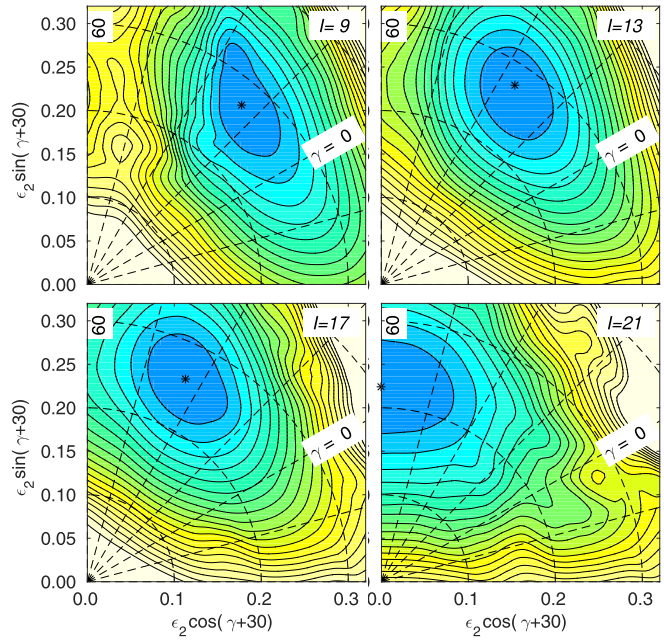

FIG. 7. Energy surfaces for spins $I = 9$, 13, 17, and 21 $\hbar$ of the $[21_+; (1_-)3_+1_+]$ configuration, which is assigned to the newly observed 1816-2221(-2607)-keV rotational sequence Q1, shown in the upper-left part of Fig. 1. Standard CNS parameters [40] were used. Contour lines correspond to energy differences of 250 keV.

a hole in the low-lying [303]7/2 Nilsson orbital at large oblate deformation.

The general features of the yrast states with standard and new parameters are very similar, where the low spin bands are formed with all valence particles in the fp orbitals followed by configurations where at first, valence particles are excited to the $g_{9/2}$ orbitals before excitations from the $f_{7/2}$ shell of the $N = Z = 28$ core become competitive in energy. Such an evolution is seen most clearly in ^{62}Zn, highlighted in Fig. 21 of Ref. [30]. Considering that pairing is not included, the difference between experiment and theory should have a spin dependence reflecting some kind of average pairing energy, i.e., of the type $c_1 \exp(-c_2 I)$ (c_1, c_2 constants), for instance, as calculated in ^{138}Nd in Ref. [48] and for ^{167}Lu in Ref. [49]. It appears that the differences using standard parameters follows such a trend somewhat better than those where the new parameters are used.

The shape evolution of the calculated $[21_+; (1_-)3_+1_+]$ configuration associated with band Q1 is shown in Fig. 7. It starts out at similarly small values of $\gamma \approx 20^\circ$ but somewhat larger prolate deformation ($\varepsilon_2 \approx 0.27$) than the $[21_+; 21_+]$ yrast structure (cf. Fig. 5 in Ref. [12]). Both structures are predicted to terminate at about the same shape at $\gamma \approx 60^\circ$, but with reversed $\varepsilon_2 \approx 0.23$ ($[21_+; (1_-)3_+1_+]$) and $\varepsilon_2 \approx 0.27$ ($[21_+; 21_+]$) quadrupole deformation. The difference in shape evolution of these two configurations can be understood from the polarizing effects of the hole in the $m = \Omega = 7/2$ or $5/2$ $f_{7/2}$ orbital. On the prolate side, a hole in the up-sloping orbitals leads to a larger deformation, while it leads to a smaller deformation on the oblate side.

VI. SUMMARY AND CONCLUSIONS

The experimental level scheme of ^{62}Ga has been extended from 10 MeV up to 17 MeV excitation energy. The onset of well-deformed rotational bands could be established in that excitation energy region reaching spin $I \gtrsim 20\hbar$. While the yrast states up to $I = 17\hbar$ are formed from the valence particles outside the ^{56}Ni core, the explanation of the higher spin states suggests one hole in the $f_{7/2}$ shell. CNS calculations with standard and new parameters provide comparable results, though details point toward a somewhat better description with the standard parameters. Any profound discussion of $T = 0$ pairing effects at high spins in ^{62}Ga calls for the identification of well-deformed [(2)32; (2)32] structures. However, a corresponding experiment will be challenging due to counteracting limitations of the required excitation energy and angular momentum versus finite absolute and sufficient relative production cross section to populate and observe ^{62}Ga at such high-lying entry states. A properly designed experiment with the next generation of γ-ray tracking arrays will be capable of handling the task [50,51].

ACKNOWLEDGMENTS

We would like to thank the accelerator crews and the Gammasphere support staff at Argonne and for their supreme efforts. This research used resources of ANL's ATLAS facility, which is a DOE Office of Science User Facility. This work is supported in part by the Swedish Research Council (Vetenskapsrådet, VR 2016-3969) and the U.S. Department of Energy under Grants No. DE-AC02-06CH11357 (ANL), No. DE-AC03-76SF00098 (LBNL), and No. DE-FG05-88ER-40406 (WU).

[1] G. F. Grinyer, P. Finlay, C. E. Svensson, G. C. Ball, J. R. Leslie, R. A. E. Austin *et al.*, Phys. Rev. C **77**, 015501 (2008).

[2] P. Finlay, G. C. Ball, J. R. Leslie, C. E. Svensson, I. S. Towner, R. A. E. Austin *et al.*, Phys. Rev. C **78**, 025502 (2008).

[3] A. Bey, B. Blank, G. Canchel, C. Dossat, J. Giovinazzo, I. Matea *et al.*, Eur. Phys. J. A **36**, 121 (2008).

[4] T. W. Henry, M. A. Bentley, R. M. Clark, P. J. Davies, V. M. Bader, T. Baugher *et al.*, Phys. Rev. C **92**, 024315 (2015).

[5] H. M. David, P. J. Woods, G. Lotay, D. Seweryniak, M. Albers, M. Alcorta *et al.*, Phys. Lett. B **726**, 665 (2013).

[6] D. Rudolph, C. Andreoiu, J. Ekman, C. Fahlander, M. N. Mineva, S. M. Lenzi *et al.*, Phys. Rev. C **69**, 034309 (2004).

[7] E. Grodner, A. Gadea, P. Sarriguren, S. M. Lenzi, J. Grębosz, J. J. Valiente-Dobón *et al.*, Phys. Rev. Lett. **113**, 092501 (2014).

[8] U. Hermkens, Ph.D. thesis, University of Cologne, 1995 (unpublished).

[9] Th. Steinhardt, Diploma thesis, University of Cologne, 1997 (unpublished).

[10] S. M. Vincent, P. H. Regan, D. D. Warner, R. A. Bark, D. Blumenthal, M. P. Carpenter *et al.*, Phys. Lett. B **437**, 264 (1998).

[11] A. L. Nichols, B. Singh, and J. K. Tuli, Nucl. Data Sheets **113**, 973 (2012); see also unevaluated data sets at https://www.nndc.bnl.gov/ensdf.

[12] A. Juodagalvis and S. Åberg, Nucl. Phys. A **683**, 207 (2001).

[13] C. E. Svensson, D. Rudolph, C. Baktash, M. A. Bentley, J. A. Cameron, M. P. Carpenter *et al.*, Phys. Rev. Lett. **82**, 3400 (1999).

[14] C. H. Yu, C. Baktash, J. Dobaczewski, J. A. Cameron, C. Chitu, M. Devlin *et al.*, Phys. Rev. C **60**, 031305(R) (1999).

[15] D. Rudolph, C. Baktash, J. Dobaczewski, W. Nazarewicz, W. Satula, M. J. Brinkman, M. Devlin, H.-Q. Jin, D. R. LaFosse, L. L. Riedinger, D. G. Sarantites, and C. H. Yu, Phys. Rev. Lett. **80**, 3018 (1998).

[16] D. Rudolph, C. Fahlander, A. Algora, C. Andreoiu, R. Cardona, C. Chandler *et al.*, Phys. Rev. C **63**, 021301(R) (2000).

[17] D. Rudolph, A. Gadea, G. de Angelis, C. Fahlander, A. Algora, C. Andreoiu *et al.*, Nucl. Phys. A **694**, 132 (2001).

[18] A. V. Afanasjev, I. Ragnarsson, and P. Ring, Phys. Rev. C **59**, 3166 (1999).

[19] O. Juillet, P. Van Isacker, and D. D. Warner, Phys. Rev. C **63**, 054312 (2001).

[20] J. Dobaczewski, J. Dudek, and R. Wyss, Phys. Rev. C **67**, 034308 (2003).

[21] S. Głowacz, W. Satuła, and R. Wyss, Eur. Phys. J. A **19**, 33 (2004).

[22] I.-Y. Lee, Nucl. Phys. A **520**, c641 (1990).

[23] D. G. Sarantites, P.-F. Hua, M. Devlin, L. G. Sobotka, J. Elson, J. T. Hood, D. R. LaFosse, J. E. Sarantites, and M. R. Maier, Nucl. Instrum. Methods Phys. Res. A **381**, 418 (1996).

[24] M. Devlin, L. G. Sobotka, D. G. Sarantites, and D. R. LaFosse, Nucl. Instrum. Methods Phys. Res. A **383**, 506 (1996).

[25] C. E. Svensson, J. A. Cameron, S. Flibotte, G. Gervais, D. S. Haslip, J. M. Nieminen *et al.*, Nucl. Instrum. Methods Phys. Res. A **396**, 228 (1997).

[26] C. Andreoiu, D. Rudolph, I. Ragnarsson, C. Fahlander, R. A. E. Austin, M. P. Carpenter *et al.*, Eur. Phys. J. A **14**, 317 (2002).

[27] L.-L. Andersson, D. Rudolph, E. K. Johansson, D. A. Torres, B. G. Carlsson, I. Ragnarsson *et al.*, Eur. Phys. J. A **36**, 251 (2008).

[28] L.-L. Andersson, I. Ragnarsson, D. Rudolph, E. K. Johansson, D. A. Torres, C. Andreoiu *et al.*, Phys. Rev. C **79**, 024312 (2009).

[29] E. K. Johansson, D. Rudolph, I. Ragnarsson, L.-L. Andersson, D. A. Torres, C. Andreoiu *et al.*, Phys. Rev. C **80**, 014321 (2009).

[30] J. Gellanki, D. Rudolph, I. Ragnarsson, L.-L. Andersson, C. Andreoiu, M. P. Carpenter *et al.*, Phys. Rev. C **86**, 034304 (2012).

[31] M. Weiszflog, G. de Angelis, A. Axelsson, D. Bazzacco, F. Becker, M. De Poli *et al.*, Eur. Phys. J. A **11**, 25 (2001).

[32] D. C. Radford, Nucl. Instrum. Methods Phys. Res. A **361**, 297 (1995).

[33] J. Theuerkauf, S. Esser, S. Krink, M. Luig, N. Nicolay, O. Stuch, and H. Wolters, program TV, University of Cologne (unpublished).

[34] J. Gellanki, I. Ragnarsson, D. Rudolph, C. E. Svensson, L.-L. Andersson, C. Andreoiu *et al.*, Phys. Rev. C **80**, 051304(R) (2009).

[35] D. Rudolph, B. G. Carlsson, I. Ragnarsson, S. Åberg, C. Andreoiu, M. A. Bentley *et al.*, Phys. Rev. Lett. **96**, 092501 (2006).

[36] C. Andreoiu, T. Døssing, C. Fahlander, I. Ragnarsson, D. Rudolph, S. Åberg *et al.*, Phys. Rev. Lett. **91**, 232502 (2003).

[37] D. Rudolph, L.-L. Andersson, R. Bengtsson, J. Ekman, O. Erten, C. Fahlander *et al.*, Phys. Rev. C **82**, 054309 (2010).

[38] R. Grzywacz, C. H. Yu, Z. Janas, S. D. Paul, J. C. Batchelder, C. R. Bingham *et al.*, Nucl. Phys. A **682**, 41 (2001).

[39] P. Ruotsalainen, C. Scholey, R. Julin, K. Hauschild, K. Kaneko, B. S. Nara Singh *et al.*, Phys. Rev. C **88**, 024320 (2013).

[40] T. Bengtsson and I. Ragnarsson, Nucl. Phys. A **436**, 14 (1985).

[41] A. V. Afanasjev, D. B. Fossan, G. J. Lane, and I. Ragnarsson, Phys. Rep. **322**, 1 (1999).

[42] B. G. Carlsson and I. Ragnarsson, Phys. Rev. C **74**, 011302(R) (2006).

[43] J. Gellanki, B. G. Carlsson, I. Ragnarsson, and D. Rudolph, Phys. Rev. C **89**, 024301 (2014).

[44] K. Pomorski and J. Dudek, Phys. Rev. C **67**, 044316 (2003).

[45] C. Plettner, H. Grawe, I. Mukha, J. Döring, F. Nowacki *et al.*, Nucl. Phys. A **733**, 20 (2004).

[46] A. Galindo-Uribarri, D. Ward, G. C. Ball, V. P. Janzen, D. C. Radford, I. Ragnarsson, and D. Headly, Phys. Lett. B **422**, 45 (1998).

[47] C. E. Svensson, C. Baktash, G. C. Ball, J. A. Cameron, M. Devlin, J. Eberth *et al.*, Phys. Rev. Lett. **80**, 2558 (1998).

[48] C. M. Petrache, I. Ragnarsson, Hai-Liang Ma, R. Leguillon, T. Zerrouki, D. Bazzacco, and S. Lunardi, Phys. Rev. C **91**, 024302 (2015).

[49] A. Kardan, I. Ragnarsson, B. G. Carlsson, and Hai-Liang Ma, Phys. Rev. C **101**, 014323 (2020).

[50] GRETA (Gamma-Ray Energy Tracking Array) Conceptual Design Report, http://greta.lbl.gov/documents (2017).

[51] W. Korten, A. Atac, D. Beaumel, P. Bednarczyk, M. A. Bentley, G. Benzoni *et al.*, Eur. Phys. J. A **56**, 137 (2020).